ACS APPLIED MATERIALS & INTERFACES

Research Article

Cite This: ACS Appl. Mater. Interfaces 2018, 10, 35705−35714

www.acsami.org

Aligning Synthetic Hippocampal Neural Circuits via Self-Rolled-Up Silicon Nitride Microtube Arrays

Olivia V. Cangellaris,[†,‡,§,∥] Elise A. Corbin,[†,§,⊥] Paul Froeter,[§,#] Julian A. Michaels,[§,#] Xiuling Li,[§,#] and Martha U. Gillette*[,†,§,∥,¶,▽]

[†]Department of Bioengineering, University of Illinois at Urbana−Champaign, Urbana, Illinois 61801, United States

[‡]Medical Scholars Program, University of Illinois College of Medicine at Urbana−Champaign, Urbana, Illinois 61801, United States

[§]Micro and Nanotechnology Laboratory and [∥]Beckman Institute for Advanced Science and Technology, University of Illinois at Urbana−Champaign, Urbana, Illinois 61801, United States

[⊥]Cardiovascular Institute, Perelman School of Medicine, University of Pennsylvania, Philadelphia, Pennsylvania 19104, United States

[#]Department of Electrical and Computer Engineering, [¶]Department of Cell and Developmental Biology, and [▽]Neuroscience Program, University of Illinois at Urbana−Champaign, Urbana, Illinois 61801, United States

Supporting Information

ABSTRACT: Directing neurons to form predetermined circuits with the intention of treating neurological disorders and neurodegenerative diseases is a fundamental goal and current challenge in neuroengineering. Until recently, only neuronal aggregates were studied and characterized in culture, which can limit information gathered to populations of cells. In this study, we use a substrate constructed of arrays of strain-induced self-rolled-up membrane 3D architectures. This results in changes in the neuronal architecture and altered growth dynamics of neurites. Hippocampal neurons from postnatal rats were cultured at low confluency (~250 cells mm^{-2}) on an array of transparent rolled-up microtubes (μ-tubes; 4−5 μm diameter) of varying topographical arrangements. Neurite growth on the μ-tubes was characterized and compared to controls in order to establish a baseline for alignment imposed by the topography. Compared to control substrates, neurites are significantly more aligned toward the 0° reference on the μ-tube array. Pitch (20−60 and 100 μm) and μ-tube length (30−80 μm) of array elements were also varied to investigate their impact on neurite alignment. We found that alignment was improved by the gradient pitch arrangement and with longer μ-tubes. Application of this technology will enhance the ability to construct intentional neural circuits through array design and manipulation of individual neurons and can be adapted to address challenges in neural repair, reinnervation, and neuroregeneration.

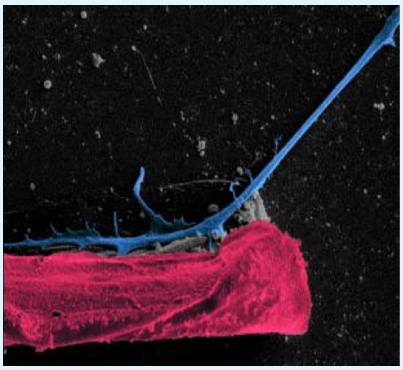

KEYWORDS: *neurons, neuronal alignment, microtubes, silicon nitride nanomembranes, self-rolled-up membranes (S-RUMs), topographical cues*

INTRODUCTION

Techniques for neuroregenerative therapies targeted to resolve neuropathologies including sensory neuropathies, or trauma-induced neurodegeneration, have gained traction through the development of techniques for precisely modulating neuronal regrowth for building-directed neural networks.[1,2] Typically, chemical,[3−5] topographical,[6−10] and electrical cues[11−14] have been used to manipulate and interrogate single cells to build synthetic neural circuitry by influencing the direction and orientation of neurite growth. Chemical cues can selectively guide axons or dendrites and polarize the orientation of neurons[3] through patterning of surface proteins, such as laminin or semaphorin 3A. Engineered topographical structures such as nanofibers or micro-channels are often used in conjunction with chemical cues to direct neurite extension due to the affinity neurons display for edges, ridges, and corners.[5−8,15−17]

Electric fields also have been used to influence the migration of neurons, accelerate neurite extension, and enhance branch complexity.[12,13] Integration of electrical signals into neuron culture was advanced through the development of multi-electrode array (MEA) technologies, which enable both neural stimulation and recording the neurons' electrical signatures within complex neural circuits.[18,19] Combining MEA technology with conventional approaches to neuron guidance, specifically topographical cues, may improve our ability to create targeted neural circuits. In this study, the topographical

Received: June 19, 2018
Accepted: September 12, 2018
Published: September 25, 2018

DOI: 10.1021/acsami.8b10233
ACS Appl. Mater. Interfaces 2018, 10, 35705−35714

cues provided by self-rolling microtubes (μ-tubes) are quantified to establish a baseline relationship prior to augmenting this technology with electric signals.

Many types of topographical cues have been utilized in the study of neurons. Positive interaction (e.g., guidance) has been observed among neurons, neurites, and topographies, which include microchannels, trenches, ridges, pillars, and tubular structures.[10,20−24] The choice of topographical signature depends greatly on the focus of the study. In this work, we utilize self-rolling μ-tubes, which provide topographical cues with unique properties to direct the response of individual neurons. Self-rolling μ-tubes are an attractive substrate because of the top-down fabrication method, which enables (1) specified control over the μ-tube position, (2) customizability of the features (e.g., diameter and structure), and (3) scalability such that many μ-tubes can be fabricated at once.[25] The diameter of the μ-tubes can be designed to allow entry of only a single neurite.[26,27] They offer the possibility of integrating a metal into the platform, enabling electrical stimulation and recording. These features make this system advantageous over traditional MEAs for studying single-cell dynamics. Previous work from our collaborators has shown the ability of μ-tubes to enhance the rate of axonal elongation compared to the rate of growth on planar regions, and qualitatively demonstrated alignment of axonal bundles of cortical neurons along the μ-tubes.[27] However, prior to coupling of electric cues to the μ-tubes, a more quantitative analysis of the interaction between the neurons and μ-tubes is required.

To effectively control neuronal alignment using the topographical cues of the μ-tube substrate, an effective substructure and related parameters must be determined and characterized. Here, neonatal rat hippocampal neurons were utilized because of their emerging complex dendritic architecture and the relatively limited understanding of dendritic development. Two methods to characterize the alignment of neuronal processes were applied. The first uses the angle of each neurite (both soma-originating neurites and branches) to provide a global analysis, which describes how the whole population of neurons responds to the μ-tube array. The second uses a defined alignment parameter based on the total length and curvature of individual neurites. This generates a measure of local alignment, that is, how the alignment of each individual neurite is affected by the μ-tube array. These results demonstrate and quantify, for the first time, the alignment properties of the μ-tube substrate with a range of organizational features. We found that, of the configurations tested, the μ-tube substrates with a gradient pitch resulted in the most effective alignment of hippocampal neurites.

MATERIALS AND METHODS

μ-Tube Fabrication. The fabrication of the μ-tube array has been reported previously; details specific to this investigation are summarized here.[25,26,28] The μ-tube array was formed on a #1.5 glass coverslip (0.16−0.19 mm thick, 22 mm × 30 mm). To start, a sacrificial layer of germanium or magnesium was deposited on the substrate using e-beam evaporation to a thickness of 20−80 nm. The low deposition rate of the sacrificial layer (1.2 Å/s) results in a high purity film with negligible surface roughness because of ripples, voids, or oxidation. Next, two layers of silicon nitride (SiN_x) were deposited using plasma-enhanced chemical vapor deposition (PECVD): the first layer with low-frequency PECVD (compressive strain) and the second with high-frequency PECVD (tensile strain) to enable strain-driven rolled-up behavior. Each layer was deposited to a final thickness of 15−20 nm, which yielded a diameter range of 4−5 μm. This parameter was chosen so that only a single neurite could enter and traverse the μ-tube.

The shape of the strained membrane was patterned by photolithography using AZ5214E and the silicon nitride bilayer was etched using Freon (CF_4) reactive ion etching, followed by the removal of the photoresist. The sacrificial layer was etched with 30% H_2O_2 at 80 °C, which released the strained membrane from the substrate, inducing spontaneous rolling from all unanchored sides.[26] The lateral etch left negligible amounts of the sacrificial layer such that the material used for the sacrificial layer did not impact neuronal growth. The high resolution scanning electron micrograph (SEM) (Figure 1A) revealed an array of μ-tubes with the silicon oxide anchor on silicon. Three μ-tube arrays were designed: (1) a standard-pitch substrate (SPμTb) with 50 μm-long μ-tubes spaced at a standard

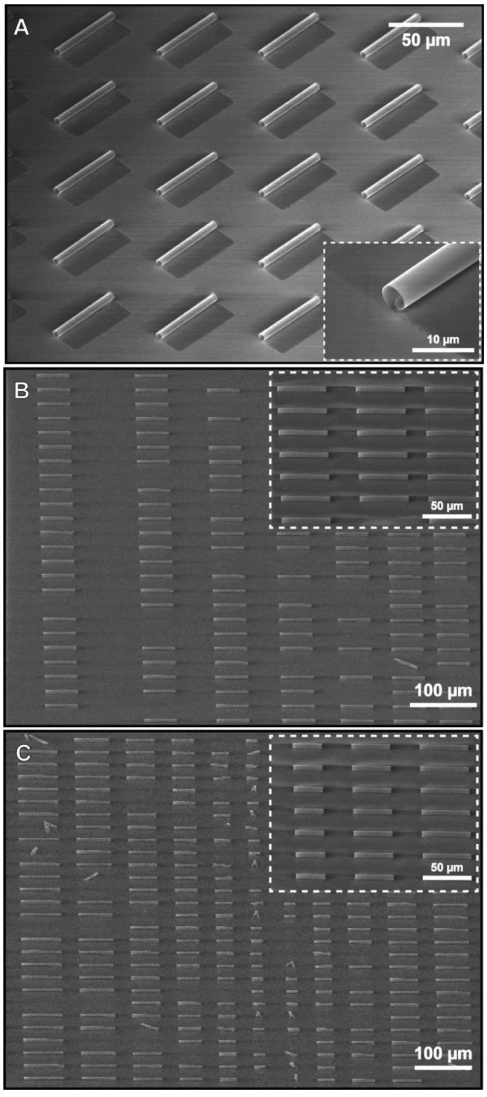

Figure 1. Scanning electron micrograph (SEM) images depict ordered arrays of μ-tubes in various configurations. (A) Standard-pitch μ-tube substrate (5 μm diameter, 50 μm length, 40 μm pitch). Inset shows magnification of a single μ-tube; (B) gradient-pitch μ-tube substrate with pitch ranging from 20−60 and 100 μm (5 μm diameter, 50 μm length). Inset shows μ-tubes separated by 20 and 30 μm pitch (right to left); (C) gradient-length μ-tube substrate with lengths ranging from 30−80 μm (5 μm diameter, 40 μm pitch). Inset shows μ-tubes with lengths 30, 40, and 50 μm (left to right). Panels (B,C) were modified in Adobe Photoshop to enhance visibility by adjusting brightness and contrast.

DOI: 10.1021/acsami.8b10233
ACS Appl. Mater. Interfaces 2018, 10, 35705−35714

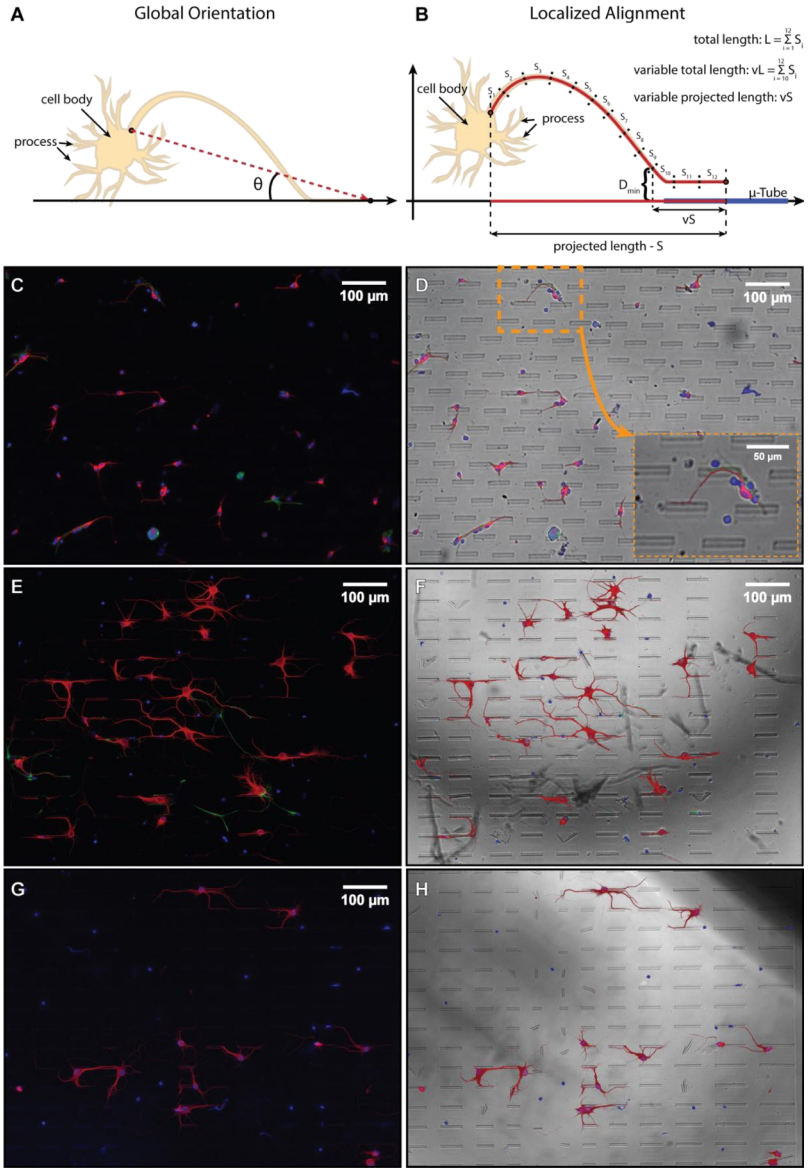

Figure 2. Analysis of relationships of neurite vs μ-tube pitch and length in developing hippocampal neurons. (A) Schematic of global orientation and alignment of a process to a μ-tube. (B) Schematic of localized orientation and alignment of a neurite to a μ-tube. Local alignment considers both the neurite length and the angle through a projection on the orientation of the μ-tube. Minimum distance (D_{min}) is determined for the variable length of a neurite as illustrated in (B). Fluorescent images of hippocampal neurons cultured on (C) standard-pitch (SPμTb), (E) gradient-pitch (GPμTb), and (G) gradient-length (GLμTb) μ-tubes and stained after 4 (SPμTb) and 7 (GPμTb, GLμTb) DIV (MAP2, red, GFAP, green, and nuclei, blue). Overlay of fluorescent image and brightfield image of neurons on (D) SPμTb, (F) GPμTb, and (H) GLμTb substrate. (D) Inset: Overlay of fluorescent image and brightfield image of a single neurite aligning to a μ-tube on the substrate. For panels C,E,G, the fluorescent images were superimposed on the brightfield image in Adobe Photoshop and saturation and color levels were adjusted to enhance contrast of neurons to improve visibility.

pitch of 40 μm across the whole chip (Figure 1A); (2) a gradient-pitch substrate (GPμTb) with 50 μm-long μ-tubes spaced at a pitch ranging from 20 to 60 and 100 μm (Figure 1B); (3) a gradient-length substrate (GLμTb) with μ-tubes of lengths ranging from 30 to 80 μm-long, separated by a static pitch of 40 μm (Figure 1C).

In order to minimize variation from the standard substrate, the μ-tube diameter was kept consistent across all substrates (4−5 μm). In the standard-pitch μ-tube array, the longitudinal and lateral pitch was constant (Supporting Information, Figure S1A). For the gradient-pitch μ-tubes, the pitch of the array varied longitudinally across a single chip (column-to-column). The lateral-pitch (row-to-row) was consistent with that of the standard-pitch array (Supporting Information, Figure S1B). For the gradient-length μ-tube array, the pitch remained fixed both longitudinally and laterally, and the μ-tubes of varying length were designed on a single chip to minimize variations, thus enabling direct comparisons (Supporting Information, Figure S1C).

Cell Culture and Preparation. Following previously established protocols, we isolated hippocampal neurons from postnatal day one or two (P1/2) Long-Evans BluGill rats, a genetically homogeneous inbred line developed by the Gillette lab.[3,29] Animals were used in accordance with protocols established by the University of Illinois Institutional Animal Care and Use Committee and in accordance with all state and federal regulations. Cells were maintained in Hibernate-A (Brain-Bits, Springfield, IL) or Neurobasal-A (Invitrogen; Carlsbad, CA) media supplemented with 0.25% GlutaMAX^{TM} (Invitrogen), 2% B-27 (Invitrogen), and 1% 100 U mL^{-1} penicillin and 0.1 mg mL^{-1} streptomycin (Sigma-Aldrich) under standard culture conditions at 37 °C during growth measurements. Neurobasal and Hibernate are

DOI: 10.1021/acsami.8b10233
ACS Appl. Mater. Interfaces 2018, 10, 35705−35714

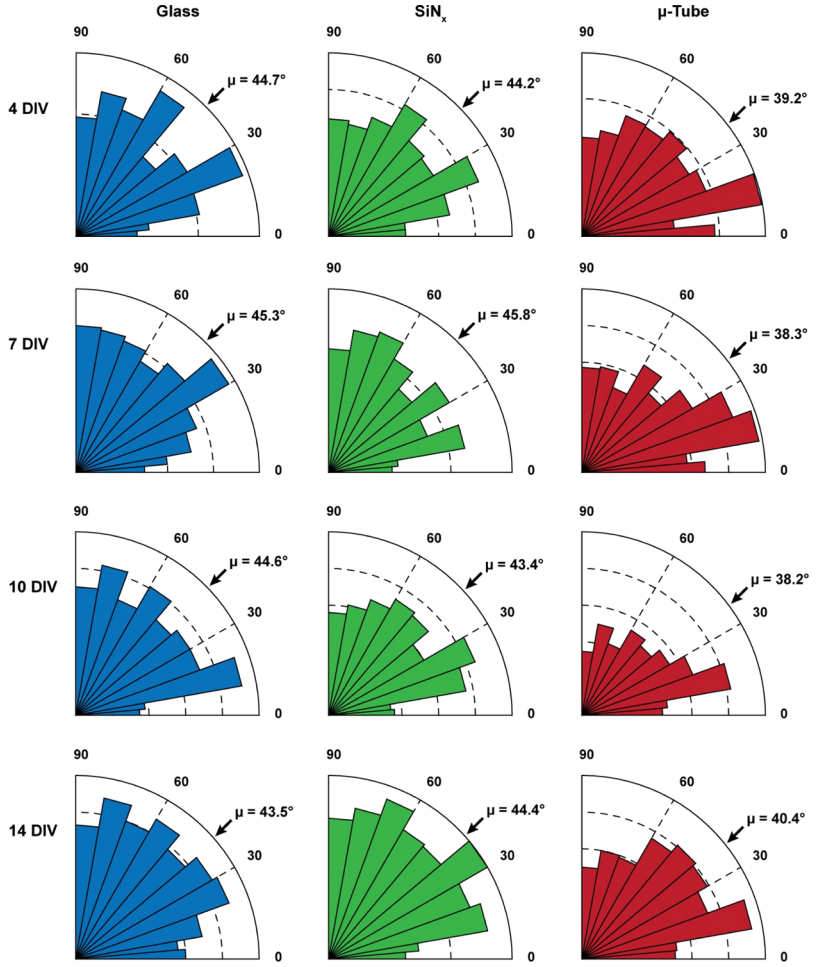

Figure 3. Quantification of global alignment considering only the angle of each neurite. Each column shows neurite angle alignment on glass, silicon nitride, and standard-pitch μ-tube substrates over 4, 7, 10, and 14 DIV. The mean angle is indicated by black arrow and corresponding μ. Neurites show significant bias toward 0° on the μ-tube substrate as compared with glass or silicon nitride. Two-way ANOVA, Tukey's posthoc test, $p < 0.0001$.

specifically developed to enhance neuronal growth in cultures of low density, as well as minimize the presence of mitotic cells.[29,30]

Following isolation of the hippocampi, the tissue was digested with papain (18.75 U mL^{-1}) 2 × 15 min, and the dissociated neurons were seeded at a density of 250 cells mm^{-2} on either the standard-pitch μ-tube substrate or one of two controls: a standard #2 glass coverslip (22 mm × 22 mm) or a standard #1.5 glass coverslip with a 40 nm thick planar bilayer of low-frequency and high-frequency PECVD SiN_x (producing the same structure as the μ-tube except not released from the substrate). Prior to cell seeding, all three substrates were coated with 0.1 mg mL^{-1} poly-D-lysine (Invitrogen). The cells were allowed to grow for 4, 7, 10, and 14 days in vitro (DIV) in a humidified incubator at 37 °C with 5% CO_2, with media changed at 4 and 7 DIV. The gradient pitch and gradient length μ-tube substrates were seeded similarly, and the cells were allowed to grow for 4 and 7 DIV in a humidified incubator at 37 °C with 5% CO_2, with media changed at 4 DIV.

Fixation and Immunocytochemistry. At the time of interest, cells were fixed (4% electron microscopy grade (EM-grade) paraformaldehyde) and cellular identities were determined using immunocytochemistry (ICC). The cells were washed with phosphate-buffered saline (PBS, pH 7.4). Following permeabilization (0.3% Triton X-100, Sigma-Aldrich), samples were blocked from non-specific antibody binding with 5% normal goat serum (Sigma-Aldrich). Then, samples were incubated with rabbit polyclonal primary antibody against neuronal microtubule-associated protein-2 (MAP2, 1:1000, Millipore Sigma), which labels early neurites and dendrites, and mouse monoclonal anti-glial fibrillary acidic protein (GFAP; 1:1000, Millipore Sigma), against glial fibrillary acidic protein, which labels astrocytic and radial glia (overnight, 4 °C). Incubation with secondary antibodies (goat antirabbit, Alexa Fluor 594 and goat anti-mouse, Alex Fluor 488) was performed (overnight, 4 °C). Finally, the cells were stained with the nuclear marker 4′,6-diamidino-2-phenylindole (1:50 000, Invitrogen). Cells were washed and stored in fresh PBS until imaging, usually within 24 h. ICC imaging was performed on a Zeiss Axiovert 100 TV fluorescence microscope. Multiple images[3−6] were taken per sample; 3 substrates were analyzed per time-point. Representative images appear in Figure 2.

Characterization of Alignment. In order to characterize the alignment of the neurites, we quantified both the relative angle of each neurite and its alignment with the orientation of the standard-pitch μ-tube array, as well as its total length. Figure 2A,B shows a general description of the approach, where neuronal processes were traced on a fluorescent MAP2 image with NeuronJ to establish the piece-wise vector of each neurite. The alignment angle was determined by taking the initial and termination points of the neurite and creating a single vector. Then, the *relative angle* was determined through comparison with the orientation vector of the μ-tube array. This simplification was used to approximate the direction of the neurite (Figure 2A). We define this determination of alignment through the use of only the neurite angle and its relation to the angle of the μ-tube array as "global alignment." For the control substrates (glass and SiN_x), where no μ-tubes were present, we chose for comparison an arbitrary angle of 0°

DOI: 10.1021/acsami.8b10233
ACS Appl. Mater. Interfaces 2018, 10, 35705−35714

relative to the image frame. Because the control substrates should not result in global alignment, any chosen angle would produce the same results.

To explore alignment beyond the global level, we evaluated the local trajectory of the process along the direction of the μ-tube. Then, coupling the projected length (S) to the total length (L), the projection was reconstructed from the piece-wise summation of the vertex points determined by NeuronJ tracings. An *alignment parameter* was defined as the squared value of the projected length divided by the total length (Figure 2B). In this way, the alignment parameter takes into account the curvature as well as the length, which enables us to derive the *localized alignment* of the neurite.

Quantifying Global Alignment. Global alignment was quantified in two ways. First, rose plots were constructed for data from each substrate (SPμTb, planar SiN_x, and glass) at each time point by pooling the angle data for each neurite (Figure 3). The symmetry of the SPμTb device allowed us to consider all neurites within a 0−90° range. The tracings acquired through NeuronJ from each fluorescent image set were used in a fast-Fourier transform (FFT) analysis to explore neurite alignment. Prior to analysis, tracings from separate images in the same set were combined to improve the diminished signal-strength inherent in low-density cultures. Images were combined in groups based on the smallest n, which in this case was 3. They were combined to enhance the coherent signals of interest (aligned neurites) and suppress the incoherent signals (random, unaligned neurites) in order to better detect these signatures through FFT analysis. For datasets with $n > 3$, combinations of 3 were created for each permutation of n to generate a common noise floor across all analyzed images. Using ImageJ, an FFT was taken for each combined image (Figure 4A) and a power spectral density (PSD) was obtained from each FFT through a radial-sums method (Figure 4B).[31] Because the image is rotated 90° when taking the FFT, the peaks of interest are shifted by 90°. A multimodal Gaussian distribution was fit to the PSD at 90° and 270° and the square of the ratio of the energy within the two peaks to the energy outside the peaks was obtained, yielding a *relative energy* for each condition and time point (Figure 4C).

Quantification of Local Alignment on μ-Tube Substrates. To define and quantify local alignment, we considered the angle in conjunction with the alignment parameter, which we previously defined as the square of the ratio of the projected length of the neurite along the direction of the μ-tube (S) to the full length of the neurite (L) (Figure 2B). *Perfect alignment* describes a neurite with an angle of 0° and an alignment parameter of 1; imperfect alignment describes a neurite with an angle of 90° and an alignment parameter of 0. However, a realistic definition of alignment requires an allowable tolerance for both the angle and alignment parameter. In order to determine the threshold for the angle and alignment parameter, we created a training set of data for each time point, in which each neurite was manually classified as aligned or unaligned, and imposed these classified points onto each histogram for 4, 7, 10, and 14 DIV (Supporting Information, Figure S2). The cutoffs for angle and alignment parameter were determined based on an average capture of 97% or better of the aligned training data. Taken together, satisfying the angle and alignment parameter cutoffs classifies a neurite as aligned.

Correlating Distance between Neurite Origin or Varied Neurite Length and μ-Tube. To explore the relationship between alignment and the relative location of a neurite to a μ-tube, we considered the minimum distance (D_{min}) between the origin of each neurite at the soma and the closest μ-tube and its relationship to the alignment of the neurite. We also considered the minimum distance between the nearest μ-tube and the point at which the ratio of the remaining projected length to the remaining total length was within a certain tolerance, greater than or equal to 0.75 (i.e. vS was at least 75% of vL). D_{min} was calculated by generating a binary image of the μ-tube array based on the brightfield image of the array, then calculating the minimum distance from each segment of each neurite to the nearest μ-tube.

For soma-originating neurites, taking the associated angle, alignment parameter, and D_{min} for each neurite, the raw D_{min} data

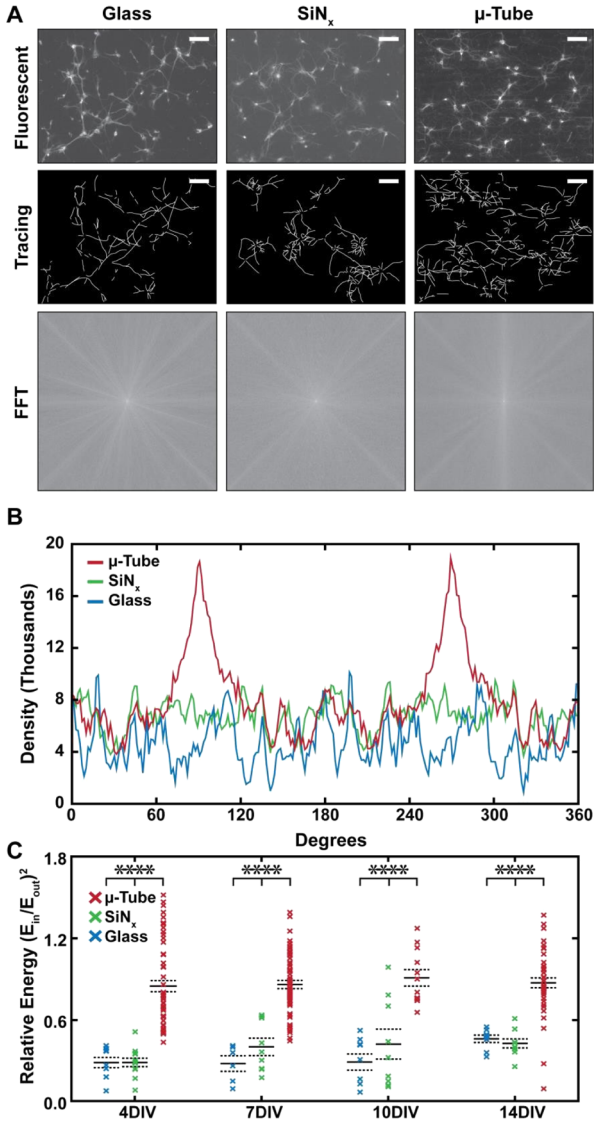

Figure 4. Quantification of the global alignment through FFT and PSD analyses reveals significant alignment of neurites with μ-tube at 90° and 270° angles. (A) Fluorescent images of neurons on glass, silicon nitride, and standard-pitch μ-tube substrates, tracings of the neurites from fluorescent images, and FFT of tracings. (B) Representative PSD shows alignment of the neurites along the direction of μ-tubes at angles 90 and 270°, whereas the other substrates do not show directional alignment. (C) Quantification of relative energies of alignment on the three substrates using Gaussian fitting to determine the energy within a peak. Relative energy on the μ-tubes compared to the two controls is significantly higher, two-way ANOVA, Tukey's posthoc $p < 0.0001$.

was limited by the angle cutoff and the alignment parameter cutoff resulting in a final set of neurites that are aligned. The unaligned neurites, or residuals, were identified as those neurites lying outside of the angle and alignment parameter cutoffs.

For the varied neurite length, working with neurites within the angle and alignment parameter cutoffs, each neurite was progressively shortened by removing segments successively beginning at the soma-origin (Figure 2B). At each variable length, the new varied projected length (vS) and the varied total length (vL) were calculated, and the ratio was evaluated. The minimum distance was isolated for all neurites, where $vS/vL \geq 0.75$ (i.e. vS was at least 75% of vL). These neurites were then progressively filtered by isolating those with a ratio greater than 0.80, 0.85, 0.90, or 0.95.

DOI: 10.1021/acsami.8b10233
ACS Appl. Mater. Interfaces 2018, 10, 35705−35714

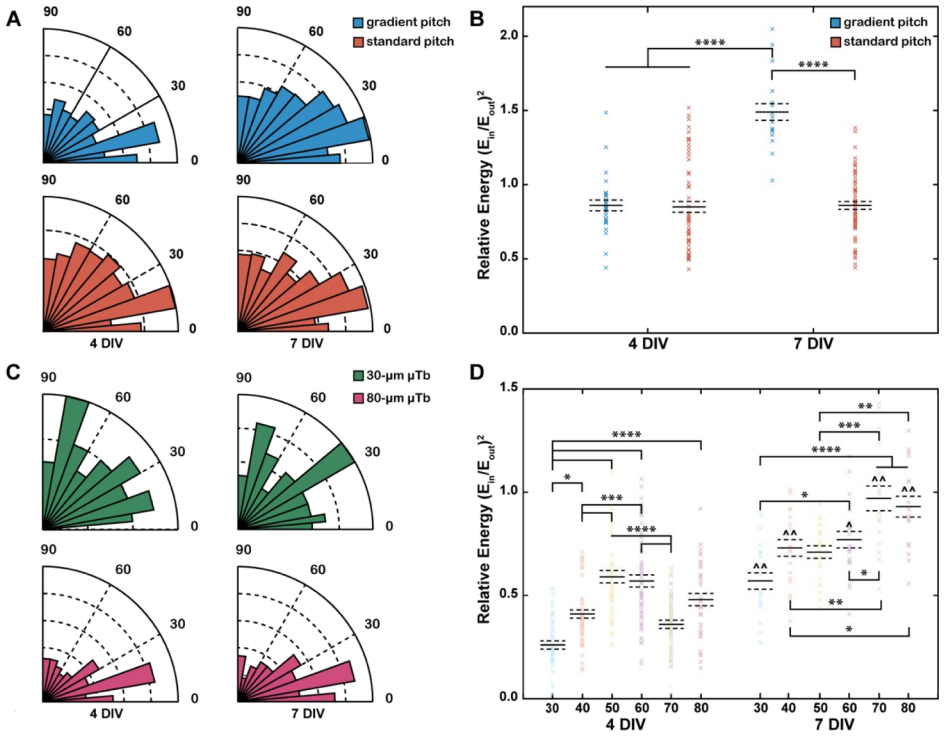

Figure 5. Global analysis of gradient substrates shows improved neurite alignment on gradient-pitch μ-tubes, and with increased μ-tube length. (A) A stronger bias toward 0° is observed for the neurite angles on the gradient-pitch μ-tube (GPμTb) substrate compared to the standard-pitch substrate (SPμTb), with a significantly smaller angle on the GPμTb (36.6° ± 0.55°) compared to the SPμTb (38.82° ± 0.48°), two-way ANOVA and Tukey's post-hoc $p = 0.0076$. (B) FFT and PSD analyzes reveal significantly higher energy on the GPμTb compared to the SPμTb at 7 DIV, and within the GPμTb substrate the relative energy is significantly higher at 7 DIV compared to 4 DIV (two-way ANOVA, Tukey's post-hoc $p <$ 0.0001). (C) Wide distribution of the neurite angles is observed with neurites on the 30 μm long μ-tubes and the angles of neurites on the 80 μm long μ-tubes show a strong bias toward 0° at both 4 and 7 DIV. 30 μm μ-tube neurites average angle 4 DIV: 43.64° ± 4.14°, 7 DIV: 40° ± 2.42°. 80 μm μ-tube neurites average angle 4 DIV: 34.29° ± 2.73°, 7 DIV: 31.44° ± 1.71°. The neurite angles were, on average, significantly smaller for neurites on the 80 μm long μ-tubes compared to those on the 30 μm long μ-tubes, two-way ANOVA, Tukey's post-hoc $p = 0.03$. (D) FFT and PSD analyzes of the gradient μ-tube length reveal significantly higher energy at 7 DIV for μ-tubes of length 60, 70 or 80 μm compared to shorter μ-tubes of length 30 μm, and significantly higher energy at 7 DIV compared to 4 DIV for all tube lengths, except 50 μm (two-way ANOVA, Tukey's post-hoc, $*p < 0.05$, $**p < 0.01$, $****p < 0.0001$, $\hat{}p < 0.01$, $\hat{}\hat{}p < 0.0001$).

Statistical Analysis. Data is reported as mean ± standard error of the mean (SEM). ANOVA was utilized for statistical analysis and Tukey's posthoc tests were performed when indicated. A p-value < 0.05 was used to determine significance.

RESULTS AND DISCUSSION

Alignment on Standard-Pitch μ-Tube Substrates. Inspection of neurons growing on the SPμTb substrate reveals instances of alignment of neurites along the edge, top, or inside the tubes; this more uniform organization of the neurites along the direction of the μ-tube array results in significant alignment compared with control images (Supporting Information, Figure S3). The scanning electron micrograph of our SPμTb design shows the arrayed geometry of the μ-tubes (Figure 1A). When the relationship of the cell geometry to the SPμTb array is compared, instances of neurites aligning with the μ-tubes are apparent (Figure 2C,D). In order to characterize the extent of alignment of neuronal processes to the μ-tube structures, we classified and quantified alignment through consideration of the neurite angle, curvature, and length. We analyzed global alignment considering the generalized approach of the angle of the neurite (Figure 2A) and localized alignment through consideration of our defined alignment parameter (Figure 2B). Additional alignment analysis relative to the μ-tube is included in the Supporting Information (Tables S1 and S2). The growth and behavior of embryonic cortical neurons on the SPμTb substrate has been reported previously, as well as the comparable viability of hippocampal neurons on both glass and SiN_x.[27]

Global alignment of the neurites was first explored by considering the pooled angles for each substrate at each time point, represented as 90° rose plots (Figure 3). Visual inspection of the rose plots on the glass and SiN_x controls suggests a wide distribution of the angles between 0 and 90°, and a bias of the angle distribution toward 0° on the μ-tubes for all time points. This observation is confirmed by a two-way ANOVA and the subsequent Tukey's posthoc test, which found significance ($p < 0.0001$) between the SPμTb substrate and each control, with no significant difference in the means of the two controls. This provides the first quantifiable evidence for enhanced alignment on the μ-tubes compared to the random growth patterns on either glass or SiN_x.

The extent of global alignment on the μ-tubes was further compared to the two control substrates via FFT and PSD analyses. Representative images of the analysis processes for each of the substrates showing the original fluorescent images, the corresponding tracings, and the processed FFT from the tracings appear in Figure 4A. Inspection of the SPμTb PSD (Figure 4B) reveals two distinct peaks at 90° and 270°, which correspond to the direction of the μ-tube array, following a

DOI: 10.1021/acsami.8b10233
ACS Appl. Mater. Interfaces 2018, 10, 35705−35714

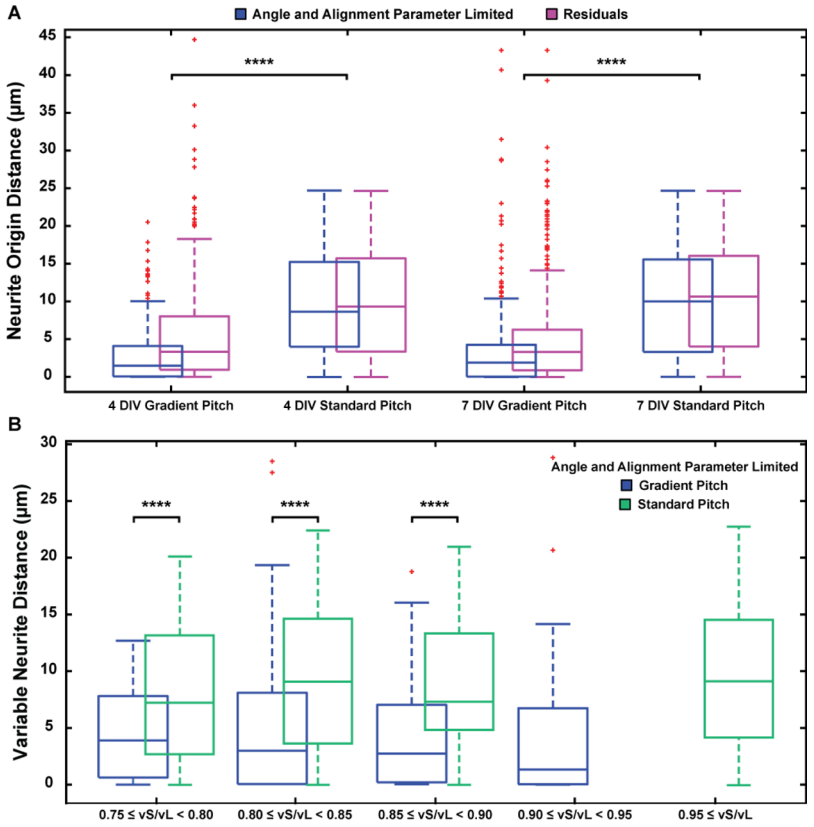

Figure 6. Neurites align more closely with μ-tubes on the gradient-pitch substrate. (A) Relationship between neurite origin distance vs alignment is presented as angle and alignment parameter limited (blue), and residuals (pink). Data are plotted for gradient- and standard-pitch μ-tube substrates at both 4 and 7 DIV. Comparison between the standard- and gradient-pitch substrates revealed significantly smaller distance between aligned neurites and the nearest μ-tube on the gradient-pitch substrate compared to the standard-pitch substrate for both 4 DIV and 7 DIV (one-way ANOVA, Tukey's post-hoc $p < 0.0001$). No significant difference was found between alignment and distance between the origin of soma-originating neurites and the closest μ-tube within the standard-pitch substrates or the gradient-pitch substrates alone (one-way ANOVA, $p > 0.05$). (B) Relationship between the minimum distance at the variable length of the neurite vs ratio of remaining projected length (vS) to remaining total length (vL). No neurites fell within the 0.90−0.95 range for the standard pitch (green), or the ≥0.95 range for the gradient pitch (blue), hence the absence of corresponding data in those regions. A significantly smaller distance was found on the gradient pitch substrate across vS/vL ratios between 0.75 and 0.90 (one-way ANOVA, $p < 0.0001$). Red crosses indicate outliers from the boxplots.

rotation of the image by 90°. The PSD for both the glass and planar SiN_x substrates (blue and green lines) shows a uniform, albeit noisy distribution, indicating that the controls again show no directional alignment over the spectra. Figure 4C shows the quantification of relative energies of alignment on the three substrates. Overall, we found that the relative spectral energy on the SPμTbs compared to the two controls is significantly higher: a two-way ANOVA and Tukey's posthoc test revealed a significant difference between the relative spectral energy of the SPμTb PSD for each time point, compared to the two controls ($p < 0.0001$). Taken together, the analyzes by rose plots and FFT power spectra confirm that the topography of the μ-tubes provides a significant cue for enhanced alignment along the direction of the array, whereas in the absence of μ-tubes, the two control substrates exhibit random neurite projections.

Tuning μ-Tube Topography to Improve Alignment. Following experiments on the standardized μ-tube array, the impact of pitch (the proximity of the μ-tubes to each other) on alignment and how the μ-tube length influenced alignment, were explored. We performed the same global and local analysis on each new substrate and compared the results from neurons cultured on the gradient-pitch μ-tube array to those on the standard-pitch μ-tube array. For the gradient-length substrates, we isolated the neurons and neurites interacting with each tube length and compared the results across the μ-tube length data sets.

Global analysis revealed that the average angle of the neurites on GPμTbs was significantly smaller than the angle of the neurites on SPμTbs (GPμTb: 36.6° ± 0.55°, SPμTb: 38.82° ± 0.48°, two-way ANOVA and Tukey's posthoc $p < 0.01$) (Figure 5A). The power-spectral density data revealed significantly higher relative energy on the gradient-pitch substrate compared to the standard-pitch substrate at 7 DIV (GPμTb: 1.49 ± 0.063, SPμTb: 0.86 ± 0.026, one-way ANOVA, and Tukey's posthoc $p < 0.0001$), with no significant difference at 4 DIV (GPμTb: 0.86 ± 0.039, SPμTb: 0.85 ± 0.04, one-way ANOVA $p > 0.05$) (Figure 5B). Additionally, while the relative energy at 7 DIV was significantly higher than at 4 DIV on the gradient-pitch substrate ($p < 0.0001$), there was no significant difference between the relative energies at 4 and 7 DIV on the standard-pitch substrate. These data suggest that over time the gradient-pitch array supports increased alignment of the neurites, compared to the standard-pitch array.

On the gradient-length substrates, a wide-angle distribution of neurites was seen on the 30 μm-long μ-tubes, with an average angle of 43.64° ± 4.14° at 4 DIV and 40° ± 2.42° at 7

DOI: 10.1021/acsami.8b10233
ACS Appl. Mater. Interfaces 2018, 10, 35705−35714

DIV, whereas the distribution of angles for neurites on the 80 μm-long μ-tubes shows a stronger bias toward 0°, with an average angle of 34.29° ± 2.73° at 4 DIV and 31.44° ± 1.71° at 7 DIV. The angles for these neurites were, on average, significantly smaller than the angles of the neurites on the 30 μm-long μ-tubes (two-way ANOVA, Tukey's posthoc $p < 0.05$) (Figure 5C). Analysis of the relative energy on the gradient-length substrate revealed two trends: (1) significantly lower energy for the shorter tube lengths (30 and 40 μm), and (2) significantly higher energy at 7 DIV compared to 4 DIV for all tube lengths except 50 μm (Figure 5D, Supporting Information, Table S3). Within the 4 DIV time-point, the highest relative energy was observed for μ-tubes with a length of 50 or 60 μm, compared to μ-tubes with lengths of 30, 40, and 70 μm. Whereas the relative energy at 7 DIV is highest for the longer μ-tubes (lengths 70 and 80 μm), in general the relative energy demonstrates an increasing trend as the μ-tubes lengthen. This difference in trend suggests that after 7 DIV, the neurites have elongated and followed the topographical cue of the μ-tubes in greater instances compared to the young neurons cultured for only 4 DIV, whose neurites are not long enough to sense the topography.

Elucidating a Relationship between Alignment and Proximity to μ-Tubes. We also evaluated the relationship between the distance separating a neuron from the nearest μ-tube and its bearing on alignment. Specifically, we considered the minimum origin distance (D_{min}) of neurites originating at the soma that was influenced by the topographic pattern of the μ-tubes in this arrayed configuration. To elucidate any relationship, we tracked how D_{min} changed between aligned and unaligned neurites over time. The boxplot (Figure 6A) reveals no significant difference in D_{min} between the aligned neurites and the unaligned neurites (residuals) on either the SPμTb array or the GPμTb array, both within individual time-points and across time. These data demonstrate that no correlation between alignment and distance between soma-originating neurites and the closest μ-tube for each configuration of μ-tubes. However, when comparing alignment and distance across the two array configurations, it is clear that the aligned neurites on the GPμTb array are separated from the nearest μ-tube by a significantly smaller distance than those found on the SPμTb array (one-way ANOVA, Tukey's posthoc, $p < 0.0001$). These data suggest that the gradient pitch provides a stronger signal for alignment to soma-originating neurites than the standard pitch. No statistical significance was found for the gradient length μ-tube array (Supporting Information).

To determine whether a specific minimum distance of the neurite from the μ-tube conferred alignment to a greater percentage of the neurite's length, an alternative location for measuring D_{min} was evaluated. Neurites were not examined based on DIV, but rather based on the vS/vL ratio, binned into one of five ranges, those with a ratio greater than 0.75, 0.80, 0.85, 0.90, or 0.95. No significant difference was found in the relationship between the distance and the vS/vL ratio for either the SPμTb substrate or the GPμTb substrate (Figure 6B). This again suggests with each configuration of μ-tubes alone, there does not exist a definitive distance at which a neurite approaches a μ-tube that will result in alignment of a larger percentage of the neurite. However, comparison between the SPμTb and GPμTb substrates reveals a significantly smaller D_{min} on the GPμTb substrate for neurites with a ratio greater than 0.75, 0.80, and 0.85 (two-way ANOVA, Tukey's post-oc, $p < 0.0001$). This indicates that, while the neurites may not exhibit differing behavior within each substrate, on the GPμTb, aligned neurites are closer to the μ-tubes than on the SPμTbs. There still appears to be no relationship between distance and percentage of the neurite that is aligned.

Overall, the data demonstrate that the μ-tube platform effectively guides neurite alignment, conferring an increased degree of order to the system well beyond the planar substrate. This understanding of the alignment of neurons-on-chip will allow for more definitive determinations regarding the influences of future μ-tube sensors independent of the coupling behavior of the base topography. This will enable elucidation of the characteristics of neurite behaviors in the presence of electric fields and overall alignment and organization of the neurons on a powered substrate.

CONCLUSION

This paper reports both the global and local alignment of hippocampal neurons on a designed μ-tube platform. We showed that the array of μ-tubes provides a strong set of cues for alignment, thereby increasing the order of the system over randomly seeded cultures on glass and SiN_x. The global alignment revealed, through both angle detection and relative energy analysis, enhanced alignment on the μ-tube substrates in the direction of the μ-tube orientation compared with control substrates. On a localized scale, gradient-pitch substrates show aligned neurites which are significantly closer to the μ-tubes. These results suggest that the best substrate for maximum alignment is the gradient-pitch substrate, likely because of the increased frequency of topographical cues. Further experiments to optimize the pitch will better elucidate this interaction. This characterization of alignment is sufficient to decouple the effects of topographic signals on neurite orientation from those of electrically or chemically induced signals. This level of discrimination positions these substrates for applications of MEA technology to design neural circuits. Furthermore, the 3D geometries provide a means to construct intentional neural circuits and also manipulate single elements within the circuit to address the grand challenges in neural repair and neuroregeneration.

ASSOCIATED CONTENT

Supporting Information

The Supporting Information is available free of charge on the ACS Publications website at DOI: 10.1021/acsami.8b10233.

> Supporting information includes a detailed description of methodology for determination of alignment parameters, representative fluorescent images of neuron growth on control substrates, supplemental data for the gradient-length μ-tube substrate for the PSD relative energy analysis and minimum distance analysis, as well as additional metrics of neuronal alignment on the experimental substrates (PDF)

AUTHOR INFORMATION

Corresponding Author

*E-mail: mgillett@illinois.edu.

ORCID

Martha U. Gillette: 0000-0003-3645-2626

DOI: 10.1021/acsami.8b10233
ACS Appl. Mater. Interfaces 2018, 10, 35705−35714

Funding

Financial support was provided in part by NSF IGERT award no. 0903622 NeuroEng (O.V.C.), the Hazel I. Craig Research Award (O.V.C.) the Medical Scholars Program at the University of Illinois and Christie Foundation Award (O.V.C.), NSF ECCS award no. 1309375 (X.L., P.F.), DOE award no. DE-FG02-07ER46471 (X.L., P.F.), and the Andrew T. Yang Research Award (X.L., P.F.), NSF STC EBICS CBET award no. 0939511 (M.U.G., O.V.C.).

Notes

The authors declare no competing financial interest.

■ ACKNOWLEDGMENTS

The authors gratefully acknowledge Curtis L. Johnson for insightful technical discussions and assistance, Jennifer W. Mitchell for discussion of statistical analysis, Anna-Liza Cangellaris for assistance in figure preparation, and Guillermo L. Monroy for thoughtful discussion and assistance with revision. The authors also thank Ann C. Benefiel for facilitating manuscript submission.

■ ABBREVIATIONS

DIV, days in vitro; D_{min}, minimum distance; FFT, fast Fourier transform; GFAP, glial-fibrillary associated protein; GLμTb, gradient-length microtube substrate; ICC, immunocytochemistry; *L*, total length; MAP2, microtubule associated protein 2; MEA, multi-electrode array; μ-tube(s), microtube(s); P1/2, post-natal day 1/2; PECVD, plasma-enhanced chemical vapor deposition; PSD, power spectral density; *S*, projected length; SiN_x, silicon nitride; SPμTb, standard-pitch microtube substrate; vL, varied/remaining total length; vS, varied/remaining projected length

■ REFERENCES

(1) McCaig, C. D.; Rajnicek, A. M.; Song, B.; Zhao, M. Controlling Cell Behavior Electrically: Current Views and Future Potential. *Physiol. Rev.* **2005**, *85*, 943−978.

(2) Lee, J. Y.; Bashur, C. A.; Milroy, C. A.; Forciniti, L.; Goldstein, A. S.; Schmidt, C. E. Nerve Growth Factor-Immobilized Electrically Conducting Fibrous Scaffolds for Potential Use In Neural Engineering Applications. *IEEE Trans. NanoBioscience* **2012**, *11*, 15−21.

(3) Millet, L. J.; Stewart, M. E.; Nuzzo, R. G.; Gillette, M. U. Guiding Neuron Development with Planar Surface Gradients of Substrate Cues Deposited Using Microfluidic Devices. *Lab Chip* **2010**, *10*, 1525−1535.

(4) Shelly, M.; Cancedda, L.; Lim, B. K.; Popescu, A. T.; Cheng, P.-l.; Gao, H.; Poo, M.-m. Semaphorin3A Regulates Neuronal Polarization by Suppressing Axon Formation and Promoting Dendrite Growth. *Neuron* **2011**, *71*, 433−446.

(5) Kwiat, M.; Elnathan, R.; Pevzner, A.; Peretz, A.; Barak, B.; Peretz, H.; Ducobni, T.; Stein, D.; Mittelman, L.; Ashery, U.; Patolsky, F. Highly Ordered Large-Scale Neuronal Networks of Individual Cells—Toward Single Cell to 3D Nanowire Intracellular Interfaces. *ACS Appl. Mater. Interfaces* **2012**, *4*, 3542−3549.

(6) Baranes, K.; Kollmar, D.; Chejanovsky, N.; Sharoni, A.; Shefi, O. Interactions of Neurons with Topographic Nano Cues Affect Branching Morphology Mimicking Neuron-Neuron Interactions. *J. Mol. Histol.* **2012**, *43*, 437−447.

(7) Baranes, K.; Chejanovsky, N.; Alon, N.; Sharoni, A.; Shefi, O. Topographic Cues of Nano-scale Height Direct Neuronal Growth Pattern. *Biotechnol. Bioeng.* **2012**, *109*, 1791−1797.

(8) Greene, A. C.; Washburn, C. M.; Bachand, G. D.; James, C. D. Combined Chemical and Topographical Guidance Cues for Directing Cytoarchitectural Polarization in Primary Neurons. *Biomaterials* **2011**, *32*, 8860−8869.

(9) Peyrin, J.-M.; Deleglise, B.; Saias, L.; Vignes, M.; Gougis, P.; Magnifico, S.; Betuing, S.; Pietri, M.; Caboche, J.; Vanhoutte, P.; Viovy, J.-L.; Brugg, B. Axon Diodes for the Reconstruction of Oriented Neuronal Networks in Microfluidic Chambers. *Lab Chip* **2011**, *11*, 3663.

(10) Li, W.; Tang, Q. Y.; Jadhav, A. D.; Narang, A.; Qian, W. X.; Shi, P.; Pang, S. W. Large-scale Topographical Screen for Investigation of Physical Neural-Guidance Cues. *Sci. Rep.* **2015**, *5*, 8644.

(11) Yao, L.; McCaig, C. D.; Zhao, M. Electrical Signals Polarize Neuronal Organelles, Direct Neuron Migration, and Orient Cell Division. *Hippocampus* **2009**, *19*, 855−868.

(12) Yao, L.; Shanley, L.; McCaig, C.; Zhao, M. Small Applied Electric Fields Guide Migration of Hippocampal Neurons. *J. Cell. Physiol.* **2008**, *216*, 527−535.

(13) McCaig, C. D. Nerve Branching Is Induced and Oriented by a Small Applied Electric Field. *J. Cell Sci.* **1990**, *95*, 605−615.

(14) Cangellaris, O. V.; Gillette, M. U. Biomaterials for Enhancing Neuronal Repair. *Front. Mater.* **2018**, *5*, 21.

(15) Millet, L. J.; Gillette, M. U. New Perspectives on Neuronal Development via Microfluidic Environments. *Trends Neurosci.* **2012**, *35*, 752−761.

(16) Leigh, B. L.; Truong, K.; Bartholomew, R.; Ramirez, M.; Hansen, M. R.; Guymon, C. A. Tuning Surface and Topographical Features to Investigate Competitive Guidance of Spiral Ganglion Neurons. *ACS Appl. Mater. Interfaces* **2017**, *9*, 31488−31496.

(17) Krumpholz, K.; Rogal, J.; El Hasni, A.; Schnakenberg, U.; Bräunig, P.; Bui-Göbbels, K. Agarose-Based Substrate Modification Technique for Chemical and Physical Guiding of Neurons In Vitro. *ACS Appl. Mater. Interfaces* **2015**, *7*, 18769−18777.

(18) Maher, M. P.; Pine, J.; Wright, J.; Tai, Y.-C. The Neurochip: A New Multielectrode Device for Stimulating and Recording from Cultured Neurons. *J. Neurosci. Methods* **1999**, *87*, 45−56.

(19) Wagenaar, D. A.; Madhavan, R.; Pine, J.; Potter, S. M. Controlling Bursting in Cortical Cultures with Closed-Loop Multi-Electrode Stimulation. *J. Neurosci.* **2005**, *25*, 680−688.

(20) Micholt, L.; Gärtner, A.; Prodanov, D.; Braeken, D.; Dotti, C. G.; Bartic, C. Substrate Topography Determines Neuronal Polarization and Growth In Vitro. *PLoS One* **2013**, *8*, 1−14.

(21) Bettinger, C. J.; Langer, R.; Borenstein, J. T. Engineering Substrate Topography at the Micro- and Nanoscale to Control Cell Function. *Angew. Chem., Int. Ed.* **2009**, *48*, 5406−5415.

(22) Nikkhah, M.; Edalat, F.; Manoucheri, S.; Khademhosseini, A. Engineering Microscale Topographies to Control the Cell−Substrate Interface. *Biomaterials* **2012**, *33*, 5230−5246.

(23) Simitzi, C.; Ranella, A.; Stratakis, E. Controlling the Morphology and Outgrowth of Nerve and Neuroglial Cells: The Effect of Surface Topography. *Acta Biomater.* **2017**, *51*, 21−52.

(24) Schulze, B. S.; Huang, G.; Krause, M.; Aubyn, D.; Bolaños Quiñones, V. A.; Schmidt, C. K.; Mei, Y.; Schmidt, O. G. Morphological Differentiation of Neurons on Microtopographic Substrates Fabricated by Rolled-Up Nanotechnology. *Adv. Eng. Mater.* **2010**, *12*, 558−564.

(25) Li, X. Strain Induced Semiconductor Nanotubes: From Formation Process to Device Applications. *J. Phys. D: Appl. Phys.* **2008**, *41*, 193001.

(26) Froeter, P.; Yu, X.; Huang, W.; Du, F.; Li, M.; Chun, I.; Kim, S. H.; Hsia, K. J.; Rogers, J. A.; Li, X. 3D Hierarchical Architectures Based on Self-Rolled-Up Silicon Nitride Membranes. *Nanotechnology* **2013**, *24*, 475301.

(27) Froeter, P.; Huang, Y.; Cangellaris, O. V.; Huang, W.; Dent, E. W.; Gillette, M. U.; Williams, J. C.; Li, X. Toward Intelligent Synthetic Neural Circuits: Directing and Accelerating Neuron Cell Growth by Self-Rolled-Up Silicon Nitride Microtube Array. *ACS Nano* **2014**, *8*, 11108−11117.

(28) Huang, W.; Yu, X.; Froeter, P.; Xu, R.; Ferreira, P.; Li, X. On-Chip Inductors with Self-Rolled-Up SiNx Nanomembrane Tubes: A Novel Design Platform for Extreme Miniaturization. *Nano Lett.* **2012**, *12*, 6283−6288.

DOI: 10.1021/acsami.8b10233
ACS Appl. Mater. Interfaces 2018, 10, 35705−35714

(29) Millet, L. J.; Stewart, M. E.; Sweedler, J. V.; Nuzzo, R. G.; Gillette, M. U. Microfluidic Devices for Culturing Primary Mammalian Neurons at Low Densities. *Lab Chip* **2007**, *7*, 987−994.
(30) Corbin, E. A.; Millet, L. J.; Keller, K. R.; King, W. P.; Bashir, R. Measuring Physical Properties of Neuronal and Glial Cells with Resonant Microsensors. *Anal. Chem.* **2014**, *86*, 4864−4872.
(31) Millet, L. J.; Collens, M. B.; Perry, G. L. W.; Bashir, R. Pattern Analysis and Spatial Distribution of Neurons in Culture. *Integr. Biol.* **2011**, *3*, 1167.

DOI: 10.1021/acsami.8b10233
ACS Appl. Mater. Interfaces 2018, 10, 35705−35714